Optimisation and control of sampling rate in localisation microscopy

Seamus J. Holden, Thomas Pengo and Suliana Manley
Laboratory of Experimental Biophysics
Ecole Polytechnique Fédérale de Lausanne (EPFL)
CH-1015 Lausanne, Switzerland
Email: suliana.manley@epfl.ch

***Abstract*—Localisation microscopy (PALM/ STORM) involves sampling sparse subsets of fluorescently labelled molecules, so that the density of bright fluorophores in a single frame is low enough to allow single molecule sub-diffraction limited localisation. The sampling rate, i.e. the density of bright fluorophores per unit time, is key to both the temporal and spatial resolution of localization microscopy. Here we present DAOSTORM, an image analysis algorithm allowing increased sampling rate, and AutoLase, an algorithm for measurement and closed-loop feedback control of sampling rate.**

I. Introduction

Localisation microscopy (PALM [1]/ STORM [2], etc.) involves two key insights. Firstly, that the positions of well separated point sources can be localized to sub-diffraction limited accuracy. Secondly, that fluorescent molecules can be made to blink in a controlled fashion under appropriate experimental conditions. By adjusting the blinking of a fluorophore such that it spends most of its time in a dark inactive state, and only a tiny fraction of its time in a bright, photon-emitting state, a single image of even a densely-labelled structure will show only a few active, well separated point sources within the image. Repeated imaging of the sample records the position of different subsets of fluorophores; by combining the many subsets of localizations obtained from multiple images, a single super-resolved image of all fluorophores within the sample may be constructed.

One of the most important parameters in localization microscopy is the sampling rate, i.e. the density of bright fluorophores per unit time. If the sampling rate is too high, the bright fluorophores will no longer be well separated, and the spatial resolution of the image will be degraded. If the sampling rate is too low, an unnecessarily large number of raw images will be required to reconstruct a single super-resolved image, reducing the temporal resolution of the measurement. Sampling rate is thus key to both the temporal and spatial resolution of localization microscopy.

Here, we focus on two key sampling problems in localization microscopy: how to increase the maximal sampling rate, and how to maintain optimal sampling rate during data acquisition.

II. Increased sampling rate by high density localization

Until recently, algorithms for localization microscopy took the following simplistic approach. All bright fluorophores within a sample are assumed to be well separated (separation much greater than FWHM of the point spread function, PSF). Then bright spots in the image are identified and fitted with a single model PSF (usually a 2D Gaussian). However, if two spots overlap even slightly, this approach fails due to the inadequacy of the fitting model, producing a single localization which is in-between the two overlapping spots. This approach only works when the imaging density (the density of bright fluorophores in a single image) is very low, severely limiting the sampling rate of the technique.

We developed DAOSTORM [3], which is capable of single molecule localization at much higher imaging density. This is achieved by simultaneously fitting multiple model PSFs to bright regions of the image, instead of just one model PSF. This simple improvement over previous algorithms allows localization at much higher imaging density, increasing the sampling rate and temporal resolution of the technique.

We compared DAOSTORM to two common "sparse" localization algorithms. "Sparse Algorithm 1" (SA1) [2] fits candidate molecules with a single Gaussian PSF of variable size and ellipticity. Localizations arising from overlapping molecules are rejected if the fitted PSF appears too elliptical ("shape-based filtering"), or too large/ small ("size-based filtering"). "Sparse Algorithm 2" (SA2) [4] fits candidate molecules with a single Gaussian PSF of fixed shape and size, without shape/ size-based filtering.

We first investigated the qualitative performance of each algorithm for images of Alexa647-labelled microtubules in fixed COS-7 cells in dSTORM photoswitching conditions [4]. The results of each algorithm on single raw images, illustrates the characteristic performance of each algorithm (Fig. 1a-c). SA1 only localized isolated molecules, which were fitted with small localization error. SA2 localized a larger fraction of the molecules, but showed large localization errors for overlapping molecules. DAOSTORM outperformed both sparse algorithms, successfully identifying almost all molecules with small localization error.

We quantified the performance of each algorithm by analyz-

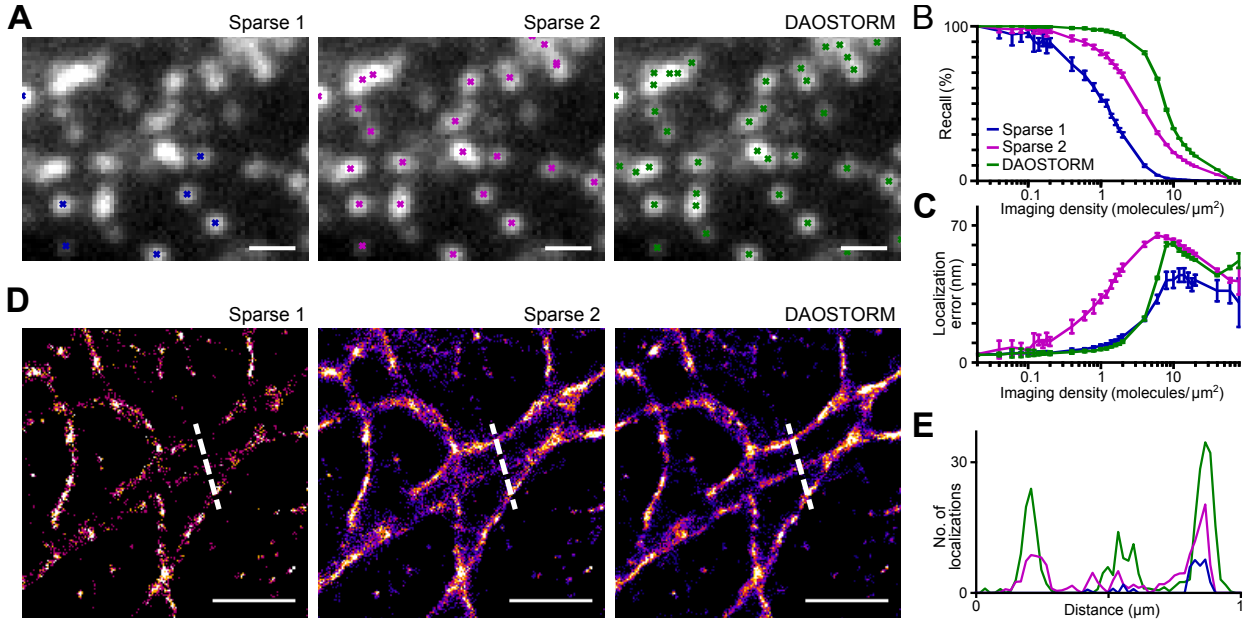

Fig. 1. *Comparison of DAOSTORM to existing super resolution localization algorithms. A.* A single image of fluorescently labeled microtubules was analyzed using SA1, SA2 and DAOSTORM. Crosses represent localizations for each algorithm. *B, C.* Recall (B) and localization error (C) of the algorithms used in a measured for simulated images of randomly distributed surface-immobilized molecules. Error bars, s.d. (n = 10). *D.* Super-resolved microtubule images from a 2000-frame data series. *E.* Line plots of cross-section indicated by dashed lines in D. Scale bars, 1 μm. Reproduced from [3]

ing simulations of randomly distributed surface-immobilized fluorophores. We compared observed localizations to simulated positions, calculating the recall and localization error at different imaging densities. The recall is the percentage of simulated fluorophores successfully detected. The localization error is the root-mean-square distance between a localization and the simulated position.

DAOSTORM substantially outperformed the sparse algorithms in simulations at high signal-to-noise ratio (SNR) typical of STORM data (Fig. 1d). SA2 gave large localization errors even at low imaging density. In contrast, DAOSTORM gave small localization errors similar to the other "precise" algorithm, SA1, together with a 6-fold improvement in recall performance.

Next, we recorded dSTORM images of the microtubule network described above, and used each algorithm to obtain super-resolved images (Fig. 1e-g). SA1 showed low recall, producing poorly sampled STORM images, while SA2 achieved higher recall, but with large localization error, leading to poorly-defined, noisy images. DAOSTORM showed high recall and small localization error, producing well-defined, low-noise images. A line-plot across three parallel microtubules demonstrates the performance difference among the algorithms (Fig. 1h): DAOSTORM resolved all three microtubules, SA2 detected two, and SA1 detected only one.

These results demonstrate the ability of DAOSTORM to increase the maximum sampling rate in localization microscopy, and thus increase temporal resolution. DAOSTORM can also increase quality of super-resolved images of biological samples in situations where control of imaging density is poor.

III. Measurement and Closed-Loop Feedback Control of Sampling Rate

During data acquisition, a careful balance in sampling rate is required: if sampling rate is too high, spatial resolution is reduced; if sampling rate is too low, temporal resolution is reduced. In both PALM and STORM, the sampling rate is usually sensitive to the illumination intensity of a "photoactivation" UV laser [1], [2]. The sampling rate can thus be adjusted to its optimal level by changing the photoactivation laser power (hereafter, UV power). However, the UV power required to maintain optimal sampling rate will vary significantly during a measurement, due to irreversible photobleaching of an increasing fraction of the fluorophores as the experiment progresses. It will also vary significantly between different fields of view within a sample, e.g. due to variations in the morphology and labelling density of the labelled structure.

Sampling rate is usually controlled by continuous manual assessment of the density of molecules in any single frame, and manual adjustment of UV power. This is tedious, and most importantly, is incompatible with automation. To resolve this, we present AutoLase, an algorithm for measurement and closed-loop feedback control of sampling rate.

A conceptually straightforwards approach [5] is to perform real-time localization analysis as the data is acquired and optimise the UV power based on the observed number of localizations. However, this approach has two serious limitations. Firstly, real-time localization is computationally intensive; this approach will therefore be difficult to implement for high frame-rate imaging and/ or for large field of view cameras

(e.g. sCMOS cameras). Secondly, and most importantly, this approach will fail at high imaging density, since multiple overlapping PSFs will be erroneously grouped together.

The design requirements for AutoLase are thus low computational burden and good performance at high imaging density. Instead of trying to optimise sampling rate using only the information from an individual frame, the problem can be significantly simplified by including temporal information from multiple frames. The amount of time that individual fluorophores remain in a bright, photon emitting state is Poisson distributed about a mean lifetime τ_{on}. Therefore, any region of a sample which remains continuously bright for significantly longer than τ_{on} very likely contains multiple bright fluorophores instead of just one. We devised an image-based estimator of τ_{on}, by estimating the amount of time that each pixel in an image has been continuously bright. This allows us to estimate the number of bright molecules, without the need for real-time localization. Since τ_{on} will increase with the number of active bright molecules, this estimator will be robust at high imaging density.

For each frame k, and for each pixel i, we define the estimated on-time, $\tau_{i,k}$,

$$\tau_{i,0} = 0,$$
$$\tau_{i,k} = (\tau_{i,k-1} + \Delta t)\ M_{th}(I_i),$$

where Δt is the interval between each frame, I_i is the intensity at the current pixel, th is an intensity threshold, and $M_{th}(I)$ is the binary threshold operator,

$$M_{th}(I) = \begin{cases} 1 & \text{if } I \geq th, \\ 0 & \text{otherwise.} \end{cases}$$

Each time the pixel intensity I_i falls below th, $\tau_{i,k}$ is set to 0. If I_i is above threshold, $\tau_{i,k}$ is equal to the duration for which that pixel has been above threshold at frame k. τ is thus a measure of how long each pixel has been *continuously* bright.

We implemented closed-loop feedback control of τ. The maximum value of τ at each frame K is smoothed via a running mean

$$\tau_{max} = \frac{1}{N} \sum_{K-N+1}^{K} \max_i\ \tau_{i,k},$$

and compared to a target value T. If the observed value of τ is above or below T by more than x %, then the UV power is reduced or increased, respectively. We calculated the image maximum of τ rather than an average, since we reasoned that the key criterion is that no region of the image contains too many active molecules.

Closed-loop feedback control was implemented on a home-built microscope, controlled using the open-source instrument control software, Micromanager [6]. We wrote a plugin to Micromanager, called *AutoLase*, to perform the feedback control, which we will shortly release as open-source software. Because Micromanager is open-source and works for a large variety of instruments, and because AutoLase is not computationally intensive and does not require real time localization analysis, it should be straightforward for researchers to implement feedback control on their own systems using our software.

The performance of the AutoLase algorithm in estimating τ_{on} is shown in Fig. 2. Live *C. crescentus* bacteria expressing FtsZ-Dendra2 [7] were imaged at a frame rate of 100 Hz using AutoLase to control the imaging density. An exemplar subset of frames (Fig. 2A) shows the blinking behaviour of the labelled molecules. Most molecules remain on for less than 100 ms, however, two molecules (top middle and top right of images) remain on for greater than 200 ms. The on-time estimator τ successfully captures this behaviour (Fig. 2B), showing only two regions active for greater than 200 ms, consistent with the visual interpretation of the raw data.

AutoLase feedback control is shown in Fig. 2C-D. With feedback control (Fig. 2C), the laser power was initially 0 %, and AutoLase was turned on at t=0 s. The raw τ_{max} data is quite noisy (grey line), but clear trends are visible in the smoothed data (black line). Before t=0 s, most molecules are in their dark state, with only occasional spikes in τ_{max} due to autofluorescence or photoactivation by the imaging laser. When AutoLase is turned on at t=0 s, the laser power (blue line) is rapidly increased and stabilises at $\sim$10 % for the first 50 s of imaging, after which point it increases in approximately exponential form to the maximum power. This produces observed on-times stable around the target value of 400 ms for nearly 100 s, after which τ_{max} gradually decreases because very few unbleached molecules remain.

Without feedback control (Fig. 2D), a new field of view (FOV) was chosen, and the laser power was set to 10 % of maximum power at t=0 s, since this was observed to be the stable initial value for the previous FOV. Interestingly, this power level produces an observed τ_{max} well above the target value of 400 ms for the first 50 s of imaging. This is presumably due to variation in density of labelled molecules between different FOVs. Between 50–100 s, τ_{max} is near the target value, after which it decreases rapidly.

These results show that AutoLase can rapidly and accurately optimise τ_{max} to a given target value, and that this value can be maintained for extended periods of time. By contrast, setting the power to a constant value without feedback control is sensitive to variations in density of labelled molecules, which occurs even between adjacent FOVs (e.g. due to variation in morphology of the labelled structure), and significantly reduces the period for which τ_{max} is close to the target value. In practice, we have found that AutoLase gives performance at least as good as manual optimisation of the UV power, while being compatible with automated imaging.

IV. Conclusions

Sampling rate is a key parameter for localization microscopy. Our algorithm, DAOSTORM, is capable of analysing localization microscopy data even at high imaging density, where many fluorescent molecules are simultaneously

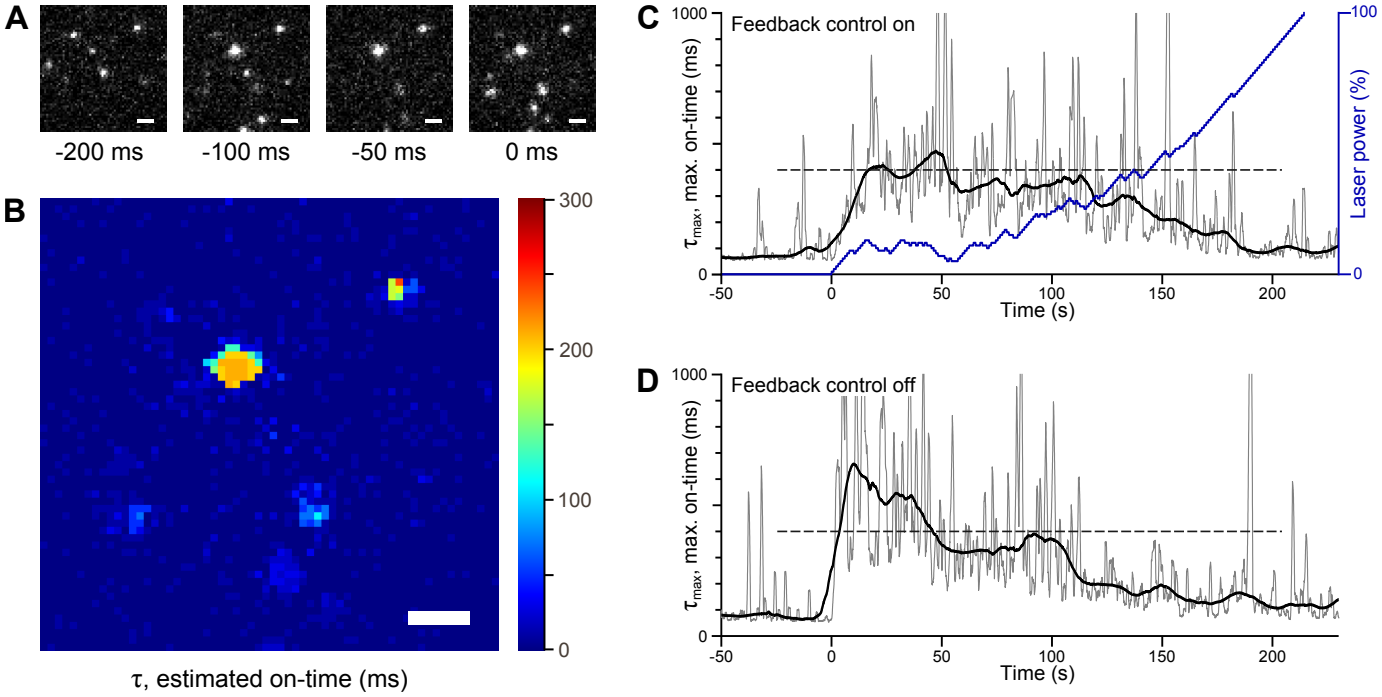

Fig. 2. *Measurement and control of molecule on-time using AutoLase*. *A.* Exemplar subset of images of live *C. crescentus* expressing FtsZ-Dendra2, under photoswithing conditions. *B.* Estimated on-time for each pixel, for frame corresponding to t= 0 ms in A. *C-D.* Observed maximum single-pixel on-time (τ_{max}) , with (C) and without (D) feedback control. Raw data, gray line; smoothed data, black line; laser power, blue line. For the case with feedback control turned off (D), UV power was set to 10 % at t= 0 s.

active. In high signal-to-noise conditions, a sixfold increase in maximum imaging density is obtained. This allows increased sampling rate with minimal loss of spatial resolution. In practice this allows super-resolved images to be constructed from fewer frames of raw data, significantly increasing the temporal resolution of the technique. These improvements are particularly useful for challenging applications such as live-cell super-resolution imaging [8].

We also presented AutoLase, an algorithm for measurement and closed-loop feedback control of sampling rate. Our algorithm is computationally non-intensive and is designed to give good performance even at high imaging density. By allowing automatic optimisation of photoactivation laser intensity, AutoLase facilitates automated localization microscopy measurements.

Acknowledgments

S.J.H and S.M. were supported by the European Research Council (grant 243016-PALMassembly). T.P. was supported by the Brazilian-Swiss Joint Research Program (grant 011004). S.J.H. was supported by a Marie Curie Intra-European Fellowship (grant 297918). We thank Erin Goley (John Hopkins University, USA) for the FtsZ-Dendra2 plasmid, and Justine Collier (University of Lausanne, Switzerland) for technical assistance.

References

[1] E. Betzig, "Imaging intracellular fluorescent proteins at nanometer resolution," *Science*, vol. 313, pp. 1642–1645, 2006.

[2] M. Rust, M. Bates, and X. Zhuang, "Sub-diffraction-limit imaging by stochastic optical reconstruction microscopy (STORM)," *Nat. Methods*, vol. 3, pp. 793–795, 2006.

[3] S. J. Holden, S. Uphoff, and A. N. Kapanidis, "DAOSTORM: an algorithm for high- density super-resolution microscopy," *Nat. Methods*, vol. 8, no. 4, pp. 279–280, Apr. 2011.

[4] S. Wolter, M. Schttpelz, M. Tscherepanow, S. Van De Linde, M. Heilemann, and M. Sauer, "Real-time computation of subdiffraction-resolution fluorescence images," *J. Microsc.* vol. 237, no. 1, pp. 12–22, 2010.

[5] A. Kechkar, D. Nair, M. Heilemann, D. Choquet, and J.-B. Sibarita, "Real-time analysis and visualization for single-molecule based super-resolution microscopy," *PLoS ONE*, vol. 8, no. 4, p. e62918, 2013.

[6] A. Edelstein, N. Amodaj, K. Hoover, R. Vale, and N. Stuurman, "Computer control of microscopes using μManager," in *Curr. Protoc. Mol. Biol* , 14.20.1–14.20.17, 2010.

[7] J. S. Biteen, E. D. Goley, L. Shapiro, and W. E. Moerner, "Three-dimensional super-resolution imaging of the midplane protein FtsZ in live caulobacter crescentus cells using astigmatism," *ChemPhysChem*, vol. 13, no. 4, pp. 1007–1012, Mar. 2012.

[8] S.-H. Shim, C. Xia, G. Zhong, H. P. Babcock, J. C. Vaughan, B. Huang, X. Wang, C. Xu, G.-Q. Bi, and X. Zhuang, "Super-resolution fluorescence imaging of organelles in live cells with photoswitchable membrane probes," *Proc. Natl. Acad. Sci. USA.*, vol. 109, no. 35, pp. 13 978–13 983, 2012.